3.4.3 *Absorption*

Extrapolating data to the 26 MHz band as given in Report 263, absorption under normal conditions will be between 0.9 and 2.2 dB and as much as 20 dB during a solar flare.

3.4.4 *Faraday rotations*

Faraday rotation of a linearly-polarized wave can be of the order of 400 revolutions at 26 MHz. Consequently, circularly polarized satellite emissions are required to avoid deep fading of signals when received using simple dipole antennas.

3.4.5 *Coverage area produced by scatter from the earth and by antenna sidelobe radiation*

In addition to a primary coverage area produced by direct illumination from the satellite, there will be, under certain conditions as illustrated in Fig. 1, a secondary area formed by scatter from the Earth's surface and consequent reflections from the ionosphere, as on ordinary Earth-Earth links [CCIR, 1982-86b].

Factors affecting this scatter propagation mode include: diurnal, seasonal and solar cycle effects on the electron density profile of the ionosphere; the geographic and geomagnetic location of the coverage area; the angle of incidence on the coverage area of the wave emitted by the satellite; and the relative roughness of the surface of the coverage area (must be sufficiently rough to generate diffuse reflections).

Preliminary calculations of the field strength were carried out using the methods described in [Chernov, 1971] for the following conditions: an illumination frequency of 26 MHz; a field strength of 60 dB(μV/m) in the coverage area; a diameter of 1000 km of the primary coverage area located at the equator; and the area is hilly, the ratio of r.m.s. height to the terrestrial irregularity correlation radius is equal to 0.05. The ionospheric conditions were taken for January, sunspot number R_{12} = 100 and 1800 h local time in the coverage area (see Report 340). The results are presented as field strength contours.

The results of the calculations for an illuminated area centred at 0° N, 20° E are shown in Fig. 2. The illustration shows that with an initial field strength of 60 dB(μV/m), the area illuminated by a scatter field strength higher than 30 dB(μV/m) is many times greater than the original area. However, to use the additional area as wanted area is difficult owing to variability of the ionosphere and fluctuating dimensions and borders of the area. This scatter effect is fairly large and may cause interference at the given frequency in adjacent areas. According to the test results [CCIR, 1986-90g] the antenna sidelobe radiation of the satellite may, in some circumstances, be quite substantial and must not be neglected.

Additional study is required to characterize statistically these effects (percentage of time and geographical extent) taking into account the factors enumerated above which affect this propagation mode.

3.5 *Example system*

The technical performance characteristics for an example system operating from the geostationary orbit are shown in Table XVI. This example is intended to highlight technical characteristics associated with a satellite system providing a good grade of service to an area with a high level of man-made noise.

3.6 *Conclusion*

Satellite and launch vehicle technology that may be used for transmission in band 7 is currently under development in the United States of America and the possibility requires examination to see whether it could lead to more effective use of the frequency spectrum. A preliminary analysis of the propagation factors indicate that systems operating in the 26 MHz band are capable of providing better than a 90% service availability during daylight hours independent of the operating period within the 11-year solar cycle. During the period of low solar activity, systems operating as low as 15 MHz may perhaps be capable of providing high availability service at night and to a lesser extent during the day.

However, further study is required before both the technical and economic feasibility of the system and its potential for achieving better frequency usage can be demonstrated.

TABLE XVI – *Link budget for geostationary sound broadcasting-satellite systems in band 7*

Operating frequency (MHz)	26
Modulation method	AM
Transmitting power (kW)	16
(dBW)	42
Satellite transmitting antenna gain (dBi)	40.2
Half-power beamwidth (degrees)	1.6
Satellite antenna diameter (m)	500
E.i.r.p (dBW)	82.2
Spreading loss (1) (dB)	−163
Absorption (dB)	−2
pfd at edge of beam (−3 dB) (dBW/m²)	−85.8
Field strength (dB(μV/m))	60
(μV/m)	1000
Polarization loss (dB)	−3
Receiving antenna gain (2) (dBi)	0
Received signal power (dBW)	−78.5
System noise figure (3) (dB)	40
Noise bandwidth (kHz)	10
Noise power (dBW)	−122.2
Carrier-to-noise ratio (dB)	43.7
Test tone-to-noise ratio in 5 kHz (4) (dB)	43.7

(1) Corresponds approximately to 20° elevation angle.
(2) Simple dipole or whip assumed.
(3) Median business area man-made noise (see Report 670).
(4) 100% modulation assumed.

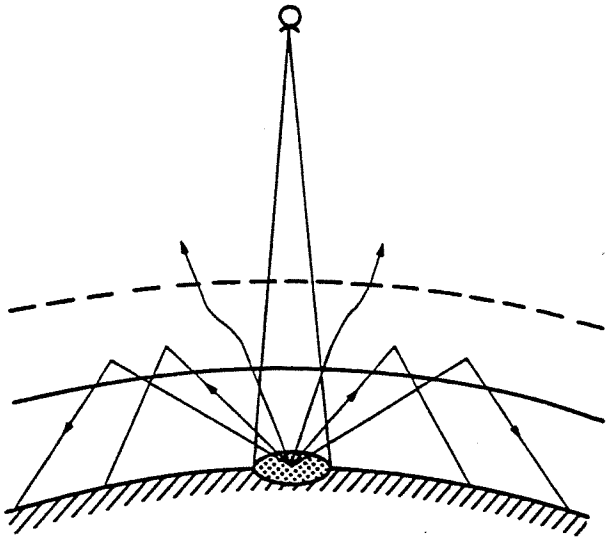

FIGURE 1 – *Area illuminated and scattering of energy*

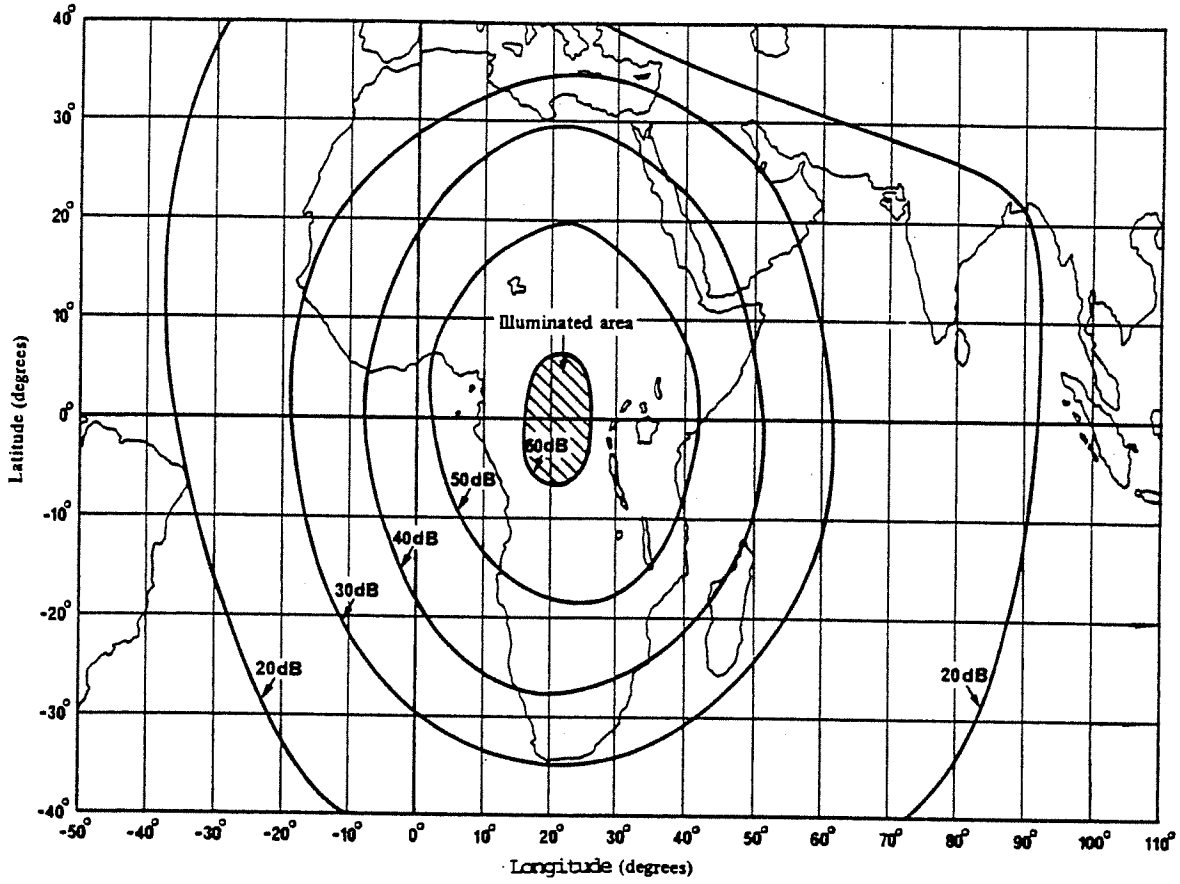

FIGURE 2 – *Calculated results for a 26 MHz transmission frequency and centre of illuminated area at 0° N, 20° E*

REFERENCES

CHERNOV, Yu. A. [1971] Vozvratno-naklonnoe zondirovanie ionosfery (Reverse oblique sounding of the ionosphere). Sviaz, Moscow, USSR.

FREELAND, R. E. [November, 1982] Survey of deployable antenna concepts. NASA Conference on Large Space Antenna Systems Technology. NASA Langley Research Centre, Hampton, Va, USA.

GUILBEAU, F. [August, 1979] Satellite sound broadcasting on frequencies of about 1 GHz. Simulation of transmissions and urban reception. *EBU Rev. Tech.*, 176, 174-178.

GUILBEAU, F. [1982] Radiodiffusion sonore par satellite, simulation d'émission à 1 GHz. Etude des fluctuations du champ en ville. Doc. TDF DX/MC/136.

PHILLIPS, G. J. and KNIGHT, P. [1978] Use of the 26 MHz band for satellite broadcasting. *EBU Rev. Tech.*, 170, 2-7.

POMMIER, D. and VEILLARD, J. [August, 1979] Etude théorique et expérimentale d'une modulation simplifiée par déplacement de fréquence d'indice ½ à phase continue. *Ann. Télécomm.*, Vol. 34, 7-8, 423-437.

POMMIER, D. and YI WU [1986] Interleaving or spectrum-spreading in digital radio intended for vehicles. EBU Rev. Tech 217.

MILLER, J.E. [1987] Technical possibilities of DBS radio at or near 1 GHz. 15th International Television Symposium and Exhibition, Montreux, Switzerland.

BALL AEROSPACE [1985] Land vehicle antennas for satellite mobile communications. Jet Propulsion Laboratory MSAT-X Report No. 108, (JPL No. 9950-1024). Ball Aerospace System Division, Boulder, Colorado, USA.

BALL AEROSPACE [1984] Concepts and cost trade-offs for land vehicle antennas in satellite mobile communication. Jet Propulsion Laboratory MSAT-X Report No. 102. Ball Aerospace Systems Division, Boulder, Colorado, USA.

CUBIC CORP. [1985] Mobile antenna and beam pointing studies for satellite mobile communications. Jet Propulsion Laboratory MSAT-X Report No. 107, (JPL No. 9950-1007). Cubic Corp., San Diego, California, USA.

CUBIC CORP. [1984] Trade-off between land vehicle antenna cost and gain for satellite mobile communications. Jet Propulsion Laboratoriy MSAT-X Report No. 103, Cubic Corp., San Diego, California, USA.

DOLBY [1985] Deltalink digital audio system. Information Sheet S85/6731. Dolby Laboratories, San Francisco, California 94111, USA.

DOLBY [1985] Instruction manual for Dolby model DP 85 digital audio encoder. Dolby Laboratories Inc., San Francisco, USA and London, England, 1984.

BULITTUDE, R.J.C., [February, 1987] Measured characteristics of 800/900 MHz fading radio channels with high angle propagation through moderately dense foliage. *IEEE Journal on Selected Areas in Communications*, SAC-5, 2, 116-128.

JONGEJANS, A., *et al*, [May, 1986] PROSAT-phase 1 report, ESA-STR 216.

LOO, C., [August, 1985] A statistical model for land mobile satellite link. *IEEE Trans. on Vehicular Technology*, 34, 3, 122-127.

LUTZ, *et al*, [May, 1986] Land mobile satellite communications - channel model, modulation and error control. *Proc. ICSDC-7*, 537-543.

PROAKIS, J.G. [1983] - Digital communications, McGraw-Hill Book Co., New York, London.

MILLER, J.E. [December 1988] - Application of coding and diversity to UHF satellite sound broadcasting systems, IEEE Transactions on Broadcasting, Vol. 34, No. 4, pp. 465-475.

ALARD, H. and LASSALLE, R. [August 1987] - Principles of modulation and channel coding for digital broadcasting for mobile receivers, EBU review No. 224, pp. 168-190.

STOTT, J.H. [1985] - Satellite sound broadcasting to fixed, portable and mobile radio receivers, BBC Report 1985/19.

ESA [1988] - Final report of the Archimedes studies; Final report of the riders concerning satellite sound broadcasting.

FTZ [1986] - System study for a Loopus satellite system - Executive summary.

CCIR Documents

[1978-82]: a. 10-11S/10 (EBU); b. 10-11S/29 (USA).

[1982-86]: a. 10-11S/152 (United Kingdom); b. 10-11S/174 (USSR).

[1986-90]: a. 10-11S/7 (JIWP 10-11/1); b. 10-11S/2 (EBU); c. 10-11S/9 (France); d. 10-11S/52 (USA); e. 10-11S/53 (USA); f. 10-11S/51 (USA); g. 10-11S/33 (USSR).

BIBLIOGRAPHY

POMMIER, D. and RATLIFF, P.A. [1988] - High-quality digital sound broadcasting for mobile, portable and fixed receivers, IBC Brighton, IEE Conference Publication No. 293.

CCIR Documents

[1978-82]: 10-11S/39 (France).

[1982-86]: 10-11S/15 (EBU); 10-11S/20 (USA); 10-11S/152 (United Kingdom); 10-11S/189 (Canada); 10-11S/213 (India); 10-11S/214 (India); 11/395 (CCIR).

ANNEX I

Satellite transmitting antenna technology

[CCIR, 1986-90a]

1. Introduction

With the relatively lower EIRP now required (see §2.6.4) which will result in a lowering of the required primary power and thus the total satellite size, it seems that the satellite antenna remains the only critical element in the realization of the space segment to provide UHF sound BSS. This annex covers the details of a number of techniques to realize the antennas and their expected performance.

Satellite-borne antennas with diameters in the range of 5 meters to 55 meters are currently in various stages of development for advanced applications such as mobile communications satellites, orbiting very-long-baseline-interferometry (VLBI) astrophysics missions, and Earth remote sensing missions [Freeland et al., 1986]. The technology being developed for these other types of applications is directly applicable to satellite sound broadcasting systems operating in band 9.

Satellite-borne antennas with diameters greater than about 3 to 4 meters must be designed so that they may be launched in a stowed configuration, and deployed once the satellite has achieved its proper orbit and has been stabilized. This constraint has led to large-aperture, reflector antenna designs based on the use of a collapsible or foldable support structure and of a light-weight, pliable, metallized mesh reflector surface.

The types of supporting structures used on the different satellite-borne antennas currently under development include the hoop/column, the tetrahedral truss, and the wrap-rib. Figure 3 shows the wrap-rib and hoop/column antennas both in the partially deployed and fully deployed stages. These deployable antennas are all of relatively light-weight and use a mesh material as the reflecting surface. In the deployed configuration, the mesh antenna surface is formed into a paraboloid either by a series of tie-points between the members of the supporting structure and the mesh (the hoop/column and tetrahedral truss antenna) or by attaching the mesh to a shaped rib (the wrap-rib antenna). The surface accuracies achieved using these shaping techniques are such that the measured radiation patterns of these developmental antennas generally conform to the co-polar reference pattern for satellite transmitting antennas given in Figure 3 of Recommendation 652.

2. SUPPORTING STRUCTURE

2.1 Hoop/Column

A 15 meter diameter hoop/column antenna has been built and tested in a ground environment [Belvin and Edighoffer, 1986]. The antenna deploys from a volume of about 1 meter in diameter by 3 meters high to a structure that is 15 meters in diameter by 9.5 meters in height. A motor driven cable system is used to deploy the antenna.

2.2 Tetrahedral Truss

A technology-demonstration 5 meter diameter tetrahedral truss antenna has been built and tested [Dyer and Dudeck, 1986]. When packaged, the overall antenna height is 1.8 meters, the truss height is 1.1 meters, the mesh diameter is 1.4 meters, and the truss diameter is 0.9 meter. The antenna is a freely deploying system that does not require motors to deploy. Deployment makes use of energy stored in the folded spring hinges (carpenter tape hinges) of the structure.

2.3 Wrap-Rib

Large-aperture, deployable reflector antennas based on the wrap-rib design use the most mature deployable antenna technology available [Naderi, 1982]. A 9.1 meter diameter version of this antenna was flown on the Applications Technology Satellite-6 (ATS-6) in 1974 [Marsten, 1975]. A preliminary design study was conducted in 1979 to characterize offset fed and axi-symmetric reflector antennas for missions requiring antennas in the 100 meter to 150 meter diameter range. The study identified critical technologies, estimated the cost and schedule required to develop the antenna, and developed a technology plan for a low-cost, low-risk "proof-of-concept" demonstration [Freeland et al., 1984].

The proof-of-concept was demonstrated in 1984, when a partial reflector was deployed in a simulated zero-gravity environment. The proof-of-concept model was a segment of a 55 meter diameter reflector consisting of a central hub (around which the ribs are wound when in the stowed configuration) and four ribs (contoured to the shape of a parabola) to which the mesh reflector material was attached. The tests demonstrated the efficacy of the deployment method and of the mesh-deployment management system.

3. REFLECTOR SURFACE

The performance of these large aperture space-borne antennas may be affected by the characteristics of the reflector material and by the accuracy of the reflector contour.

3.1 Effects of the Wire Mesh

A knitted wire mesh is the reflector material of choice for each of the antenna types cited. A typical mesh is a tricot knit of 0.003 cm diameter gold-plated molybdenum wire with about 3 openings per centimeter. An analysis to determine the effects of the knitted wire mesh on the gain, side lobe, and cross-polarization performance of large-aperture antennas has been performed [Rahmat-Samii and Lee, 1985]. It was shown that the performance of the mesh reflector antenna should be comparable to that of a solid reflector antenna when the geometry of the mesh material was properly selected (i.e., by properly selecting the opening size relative to a wavelength, rectangular vs. square openings, and the orientation of the rectangular opening relative to the incident polarization vector). Specifically, side lobes in excess of 30 to 35 dB below the level of the main beam were achievable using a pliable, light-weight, wire mesh reflector material.

3.2 Surface Accuracy

The hoop/column and the tetrahedral truss antennas use tie-points to connect the mesh surface to the support structure and to form the surface into a parabolic shape. It was found that grating lobes were generated in the far-field pattern by periodic "pillowing" of the surface, which was in turn, caused by errors in "tensioning" the uniformly spaced tie-points. When the placement of the tie-points was randomized, the grating lobes were no longer evident [Bailey, 1986]. Figure 4 illustrates the measured performance of an offset-fed, 5 meter tetrahedral truss antenna operating at a scale frequency of 4.26 GHz [Dyer and Dudeck, 1986]. It is noted, that this performance should scale to a 20 meter diameter antenna operating at a frequency around 1 GHz.

The achievable surface accuracy of the wrap-rib antenna has also been studied. This antenna design relies on both the accuracy and on the thermal characteristics of the rib cross-section to define the reflector surface formed by the mesh. Studies of the performance of a 20 meter diameter wrap-rib antenna in a space environment indicate that an rms surface accuracy of 3 mm can be achieved [Freeland, 1987]. This corresponds, for example, to an rms surface accuracy of $\lambda/100$ at an operating frequency of 1 GHz; a value that will ensure low side lobes.

4. IN-ORBIT TESTS

In order to verify that these large aperture deployable antennas will perform as required in a space environment, it is necessary to test them in an environment that simulates, as closely as possible, the zero-gravity and thermal vacuum conditions found in outer space. Ground testing of these antennas, even when suitable facilities exist, is extremely difficult and expensive, and frequently yields results of questionable value. A flight test of a high-performance, low-side lobe, 20 meter diameter wrap-rib prototype antenna system on the Shuttle or on another suitable vehicle is being studied as a means to significantly reduce the risk and uncertainty associated with the operational use of an antenna and to provide the added benefit of helping to validate ground test procedures for future antenna systems [Freeland et al., 1986; Freeland, 1987].

5. SUMMARY AND CONCLUSIONS

There is significant work underway to develop high-performance, deployable, light-weight, space-qualified reflector antennas with diameters ranging from 5 meters to over 55 meters and which exhibit sidelobe levels on the order of 30 dB or more below the peak gain of the antenna. Axi-symmetric and offset-fed antennas are being developed. A tricot knit, gold-plated molybdenum wire mesh is used for the reflecting surface. Analyses, confirmed by experiment, show that a properly chosen wire mesh reflector surface will not degrade the antenna performance in the sidelobe region. When this condition is met, the antenna performance in the sidelobe region is primarily determined by the mechanical deviations of the reflector surface from a paraboloid. During the course of developing the tetrahedral truss antenna, it was found that random positioning of the tie-point locations was an effective means by which to eliminate the grating lobes exhibited by antennas that use regularly spaced tie-points.

The difficulties associated with space-qualifying these large-aperture deployable antenna structures using ground testing has led to the study of using flights of the Shuttle or other suitable vehicles to perform the requisite qualification tests. In-orbit testing of a high-performance, 20 meter diameter wrap-rib antenna is being studied.

It may be concluded on the basis of the on-going work cited in this contribution that the satellite transmitting antenna radiation pattern given in Figure 9 of Annex 5 to Appendix 30 (ORB-85) is a viable reference radiation pattern to use for sharing studies and for system studies involving satellite sound broadcasting systems operating in band 9.

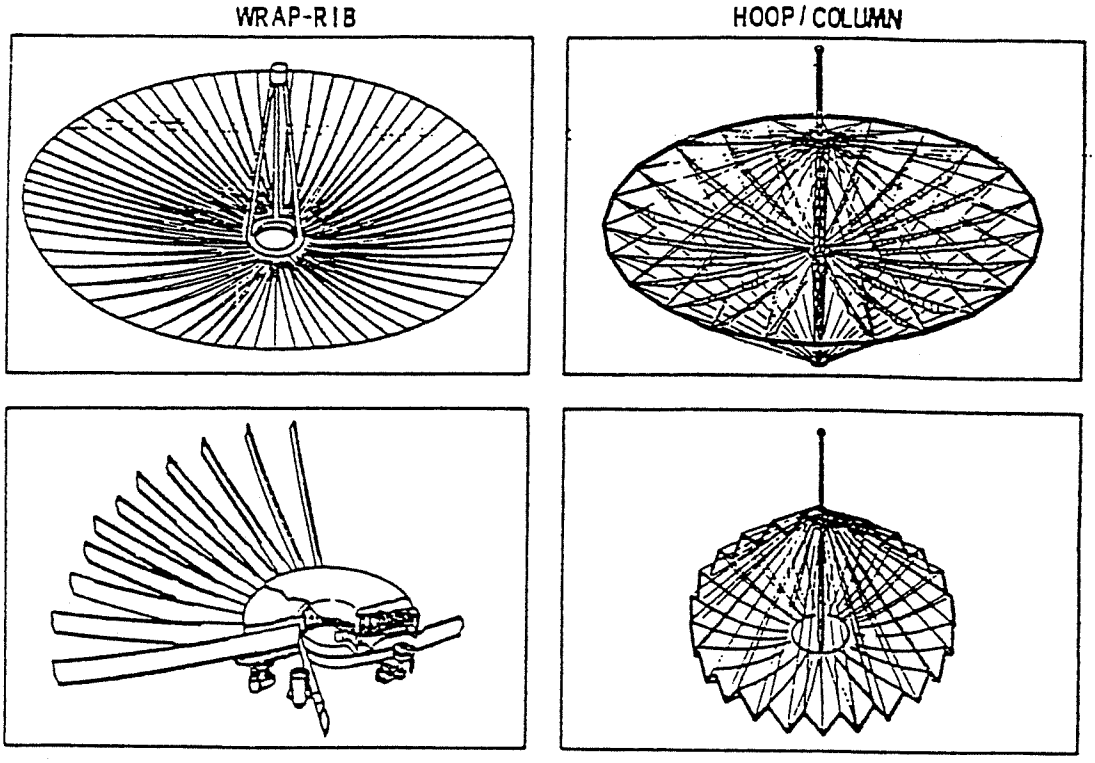

Figure 3 - Partially and fully deployed wrap-rib and hoop/column antennas [Jordon et al, 1984].

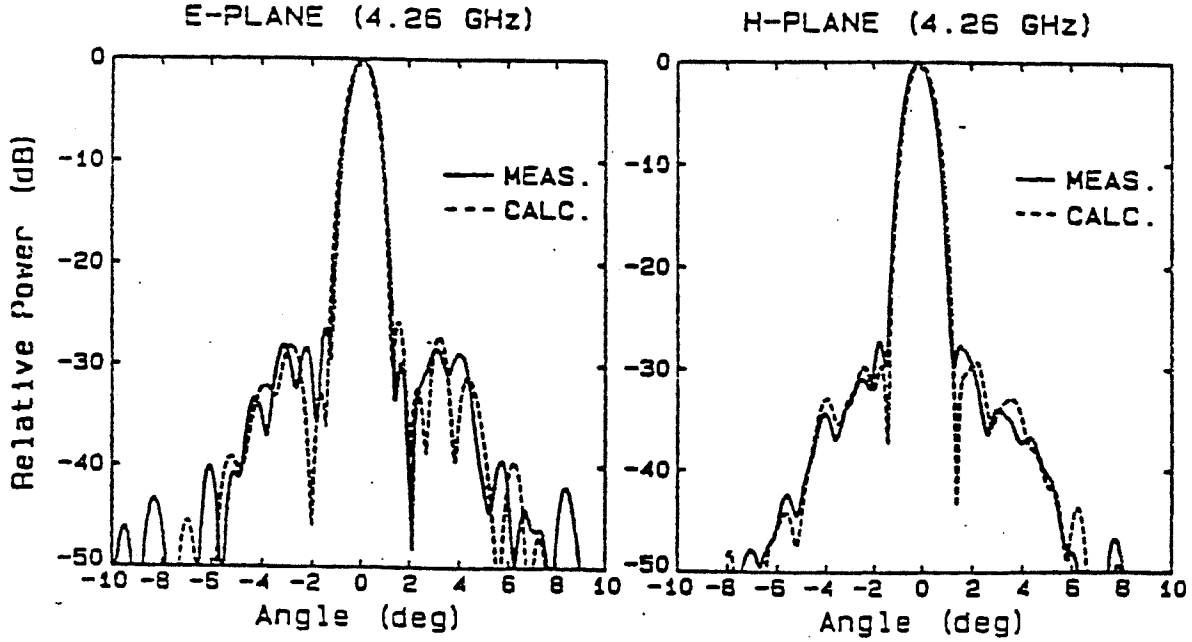

Figure 4 - Comparison of the calculated and measured antenna pattern of a 5 meter tetrahedral truss antenna operating at 4.26 GHz [Bailey, 1986].

REFERENCES

BAILEY, M.C. [1986] Hoop/Column and Tetrahedral Truss Electromagnetic Tests, Proceedings of NASA/DOD Control/Structures Interaction Technology Conference, NASA Conference Publication 2447, pp 737-746

BELVIN, W.K. and EDIGHOFFER, H.H. [1986] 15 Meter Hoop-Column Antenna Dynamics: Test and Results, Proceedings of NASA/DOD Control/Structures Interaction Technology Conference, NASA Conference Publication 2447, pp 167-185

DYER, J.E. and DUDECK, M.P. [1986] Deployable Truss Structure Advanced Technology, Proceedings of NASA/DOD Control/Structures Interaction Technology Conference, NASA Conference Publication 2447, pp 111-124

FREELAND, R.E. [10-17 October 1987] Mobile Communication Satellite Antenna Flight Experiment Definition, 38th Congress, International Astronautical Federation, Paper IAF-87-314, Brighton, England

FREELAND, R.E., GARCIA, N.F., and IWAMOTO, H. [1984] Wrap-Rib Antenna Technology Development, Proceedings of the Large Space Antenna Systems Technology Conference, NASA Conference Publication CP-2368, pp 139-166

FREELAND, R.E., METTLER, E., MILLER, L.J., RAHMAT-SAMII, Y., and WEBER III, W.J. [1986] Antenna Technology Shuttle Experiment (ATSE), Proceedings of NASA/DOD Control/Structures Interaction Technology Conference, NASA Conference Publication 2447, pp 779-807

JORDON, J.F., FREELAND, R.E., LEVY, G.S. and POTTS, D.L. [1984] QUASAT-An Orbiting Very Long Baseline Interferometer Program Using Large Space Antenna Systems, Proceedings of the Large Space Antenna Systems Technology Conference, NASA Conference Publication CP-2368, pp 117-125

MARSTEN, R.B. [November 1975] ATS-6 Significance, IEEE Transactions on Aerospace and Electronic Systems, Vol. AES-11, No. 6, pp 984-993

NADERI, F. editor [February 15, 1982] Land Mobile Satellite Service (LMSS): A Conceptual System Design and Identification of the Critical Technologies, Part II: Technical Report, NASA Jet Propulsion Laboratory Publication 82-19

RAHMAT-SAMII, Y. and LEE, S-W [January 1985] Vector Diffraction Analysis of Reflector Antennas with Mesh Surfaces, IEEE Transactions on Antennas and Propagation, Vol. AP-33, No.1, pp 76-90

CCIR Documents

[1986-90]: 10-11S/53 (USA).

ANNEX II

Propagation characteristics and link margins of the UHF satellite channel

[CCIR, 1978-82a, b, c] [CCIR, 1986-90a]

1. Introduction

Satellite sound broadcasting to portable and mobile receivers is different in several respects from its terrestrial counterpart. On the other hand, there are some similarities with satellite land-mobile communications.

Previous studies by the EBU [CCIR, 1978-82d] and the United States [CCIR, 1978-82e] considered specific examples of link budgets and link margins for certain angles of elevation, conditions of reception and other parameters. Two specific methods have been suggested and various aspects are analyzed and compared in section 3 of this annex.

The recent experiments have shown substantial agreement with the signal power distribution functions for large and small area (see section 2). In the light of the European experimental programme [Jongejans, 1986], a new composite propagation model is proposed. This model combines both the small area Rice/Rayleigh probability function and the large area log-normal probability distribution.

The design of suitable modulation systems for the type of broadcasting service will rely on propagation statistics relating to time-delay spread and correlation bandwidth of the transmission channel. These concepts, together with other related topics, have not been previously discussed in Report 955; they are now presented in section 4 of this annex, together with the recent experimental data.

2. Propagation models

The probability distribution functions relevant to the reception of satellite signals were found to correspond to a number of statistical distribution models related to the specific environment. These distribution models are generally different in so-called "small areas" and "large areas". The former are usually defined as locations extending over a number of wavelengths (for example over 40 wavelengths resulting in a distance of about 10 m). The latter extend over several small areas.

2.1 Large area distribution function

On large areas, it has been found experimentally [Guilbeau, 1979; Hess, 1980; Lutz, 1986, Jongejans 1986], that the probability distribution function of the mean received signal power takes the log-normal form:

$$P_{LN}(S_o; \mu, \sigma) = (K/(S_o\,\sigma)) \exp\left[\left(-1/2\right)\left((L_{So} - \mu)/\sigma\right)^2\right], \quad K = 10/(\sqrt{2\pi}\ln 10) \qquad (1)$$

where:

So(W): mean received signal power over a small area;

$\bar{S}_f$(W): mean received signal power over a large area under free space propagation conditions;

L_{So}(dB) = 10 log(So/$\bar{S}_f$, level of So relative to free space level;

μ(dB) = mean of L_{So} over a large area;

σ(dB) = standard deviation of L_{So} over a large area.

In equation (1), the mean value and the standard deviation are both expressed in terms of dB, relative to the free-field power level, in order to facilitate comparison between the theoretical model and measured data.

The large area model given above was experimentally verified and confirmed by [Lutz *et al*, 1986] and [Jongejans *et al*, 1986]. Using the same notation as in equation (1), the following parameter values were measured (see Table XVII).

TABLE XVII - *Measured large area parameters for various* environments

Environment	Antenna	μ_{sh}(dB)	σ_{sh}(dB)	CF	μ_{los}(dB)	$(C/M)_{los}$(dB)
Urban	C3	-10.7	3.0	0.60	-1.8	3.0
	D5	-12.2	4.4	0.78	-4.9	9.3
	S6	-12.9	5.0	0.79	-5.2	11.9
Woods	C3	-9.3	2.8	0.59	-2.7	9.9
	D5	-5.3	1.3	0.54	-1.8	10.7
	S6	-5.8	1.1	0.56	-2.1	12.9
Highway	C3	-7.7	6.0	0.25	-0.4	11.9
	S6	-7.0	4.8	0.23	-0.6	18.3

where:

μ_{sh}(dB)	:	μ in shadowed areas,
μ_{los}(dB)	:	μ in non-shadowed (line-of-sight) areas,
σ_{sh}(dB)	:	standard deviation of S_o in shadowed areas
CF	:	clutter factor, defined as the proportion of the time for the direct path being obstructed assuming a constant vehicle speed
$(C/M)_{los}$(dB)	:	ratio of direct (carrier) signal to the diffuse multipath power in non-shadowed (line-of-sight) areas
C3	:	hemispherical pattern, 3 dBi gain
D5	:	toroidal pattern, 5 dBi gain
S6	:	toroidal pattern, 6 dBi gain

Several points may be deduced from Table XVII:

- The measured average power levels in shadowed areas are very much less than those in non-shadowed areas in the same environments; for example, in urban zones the additional attenuation due to shadowing may be as high as 9 dB, in the woods 6.5 dB and on highways 7 dB. It follows that the main problem in providing a service is to overcome shadowing effects.

- The influence of the type of the receiving antenna seems to be quite significant especially on the ratio between the direct component and the multipath power in the non-shadowed areas.

- In urban areas, the shadowing loss is proportional to the antenna gain. Standard deviation, σ, and C/M ratio are proportional to the antenna gain. This last fact may be significant in the design of digital modulation systems for reception in urban areas.

In the European experiment simulation of the satellite transmission conditions were created by positioning the transmitting antenna on the Eiffel tower in Paris and measurements were made at a frequency of 839 MHz and for an average elevation angle of 25° [Guilbeau, 1979]. From this reference one can extract the parameters for equation (1). Table XVIII lists these parameters together with the values predicted from US data for the frequency of 839 MHz and an elevation angle of 25°. The values of the PROSAT expriment are derived from Table II.

TABLE XVIII

Urban zone			
Parameters of log-normal distribution for urban areas	Average	Obstructed visibility	Direct visibility
μ (dB) Guilbeau	-7.5	-11.5	-0.7
(USA)	-6.3	-10.1	-2.6
PROSAT	-6.3	-10.7	-1.8
σ (dB) Guilbeau	3.2	2.9	2.0
(USA)	3.7	4.3	3.1
PROSAT	-	3.0	-

From this table it can be seen that reasonable agreement exists between the three experiments.

Measurements made with the ATS-6 satellite in the United States [Hess, 1980] provide values for μ and σ for different areas under different receiving conditions. From the above reference a simple method for the assessment of μ and σ can be derived as follows:

$$\mu = -[A + 1.93\ f - 0.052\ \delta] \quad (2)$$

$$\sigma = 1/2\ [B + 0.053\ f + 0.040\ \delta] \quad (3)$$

where the parameters μ, σ, $\bar{S}_o$ and $\bar{S}_f$ are defined in Equation (1), and

f: frequency (GHz)

δ: elevation angle (degrees)

Values for A and B are given in Table XIX for different receiving conditions. In the Table direct visibility indicates instances where the streets in the urban area are running parallel to the satellite azimuth and obstructed visibility is on streets running perpendicular to the satellite azimuth combined with the unfavourable side of the street.

TABLE XIX

	Urban zone			Suburban/rural zone		
	Average	Obstructed visibility	Direct visibility	Average	Obstructed visibility	Direct visibility
A(dB)	6.0	9.8	2.3	1.1	5.1	0.5
B(dB)	6.4	7.6	5.2	1.1	2.4	-

These values were partially derived from [Hess, 1980] by extrapolating with the assumption that sensitivities were 0.1 dB/percent for rural and 0.2 dB/percent for urban areas, below the specified 90% coverage level. They were confirmed by the European experiments [Lutz and Jongejans ,1986] for urban areas and woods. However, this modelling does not seem to be appropriate for the non-shadowed highways.

2.2 Small area distribution functions

The recent European [Jongeans,1986] and United States' data indicate that the small area behaviour of the received signal can be modelled by a Rician distribution (constant vector plus Rayleigh distributed vectors).

If the ratio of direct signal power C to the diffuse multipath signal power M is denoted as C/M, the envelope probability distribution in an isolated small area is given by equation (4):

$$p(r) = (r/M)(\exp(-r^2/2M - C/M) \cdot I_o [r \sqrt{2C/M}] \qquad (4)$$

The parameter C/M is important as a measure of fading characteristics* of the channel. If C/M is high, the envelope probability distribution p(r) approaches a Gaussian distribution with mean $\sqrt{2C}$ and standard deviation $\sqrt{M}$. If C/M is low, p(r) approaches a Rayleigh distribution since: the modified Bessel function of first kind zero order

$$I_o(z) = \sum_{n=0} z^{2n}/2^{2n}(n!)^2 = 1 + z^2/4 + \ldots$$

approaches 1 as z approaches 0.

The corresponding probability density of $y = \frac{r^2}{\overline{r^2}}$ is given by:

$$P_R(y) = (C/M + 1) \exp[-y(C/M + 1) - C/M] \cdot I_o [2\sqrt{y(1 + C/M)C/M}] \qquad (5)$$

where:

$$y = r^2/\overline{r^2} = r^2/s_o$$

* The time intervals with received power level below a certain threshold are called fades.

The level crossing rate (LCR) at the level V is given by equation (6):

$$LCR = \frac{b}{\sqrt{2\pi}} p_R(V) \qquad (6)$$

where $p_R(V)$ is the envelope of the Rice probability density function at the value V, and b is the function of magnitude and the frequency content of the multipath reflections:

$b = 2\pi^2 B_d^2 . M$, where B_d is a Doppler spread.

Equation (6) shows that the level crossing rate and probability density function are closely linked. Therefore, the parameter C/M of $p_R(y)$ can be determined through the measurement of LCR.

The average fade duration (AFD) at the level V is given by:

$$AFD = (1/LCR) \int_0^V p_R(r)\, dr \qquad (7)$$

AFD is an important factor in designing a digital transmission system which should be designed in such a way that it overcomes long fades using a complex interleaving system.

The validity of the Rice model has been demonstrated by the PROSAT experiment on the basis of a composite log-normal - Rice mode (see §2.3).

Some typical average values of C/M for non-obstructed visibility are given in Table XVII (see §2.1). Since C/M is the only parameter $p_R(y)$ given by equation (5), the Rice probability function $p_R(y)$ is fully characterized if C/M is known.

In [Jongejans, 1986] some typical values of LCR and AFD at mean envelope level are given for vehicle speed 30 km/h. They are reproduced in Table XX below:

TABLE XX - The LCR and AFD values in different environments

	LCR (Hz)	AFD (ms)
Open area	30	20
Suburban	14	40
Rural	16	33

2.3 *The combined propagation model*

European researches [Jongejans, et al, 1986] and [Lutz, 1986] concluded that the probability density function of the received power should combine log-normal and Rice (Rayleigh) distribution in order to take account of both large-area variations and small-area variations. The distribution of instantaneous values in a small area is obtained by considering a Rice or Rayleigh variable whose mean value is itself a random variable having a log-normal distribution. The combined distribution of the received power S may be described as shown in equation (8):

$$P(S) = CF \int_0^{S_m} P_r(S,So)\, P_{LN}(So)\, dSo + (1-CF) \int_{S_m}^{S_M} P_R(S,So)\, P_{LN}(So)\, dSo \qquad (8)$$

where:

S_o : average received signal power over small area ($S_o = C + M$)

$p(S)$: combined distribution density function of the instantaneous received power in a small area

$P_r(S,So)$: Rayleigh distribution over obstructed (shadowed) small areas

$P_{LN}(So)$: distribution of mean power of small areas distributed over a large area

Sm : maximum obstructed power over a large area concerned

$P_R(S,So)$: Rice distribution over nobstructed (renshadowed) small areas

S_M : Maximum line of slight power over a large area concerned

CF : clutter factor, defined as the proportion of the time for the direct path being obstructed assuming a constant vehicle speed.

Figures 5a) and 5b) show complementary cumulative probability distribution functions of the normalized received power on highway and in city environments [Lutz *et al*, 1986]. The two figures are plotted on a Rayleigh scale. The full lines represent the theoretical channel model. Statistics of the recorded channel obtained by the measurements are designated as dots.

Three parts of the curves can be distinguished. At low values of the received power, the curve slope approximates the slope of the straight diagonal line which corresponds to a Rayleigh distribution; thus this part of the curve has clearly Rayleigh characteristics. At high values of received power, the slope of the curve indicates a Rice distribution; on highways, the Rice law is followed in 80% of small areas whereas in city environments it applies in 20% of small areas. The central part of the curves follows a log-normal law.

Similar results have been obtained [Jongejans *et al*, 1986]. They all demonstrate very good compliance between the theoretical models and the measuring results.

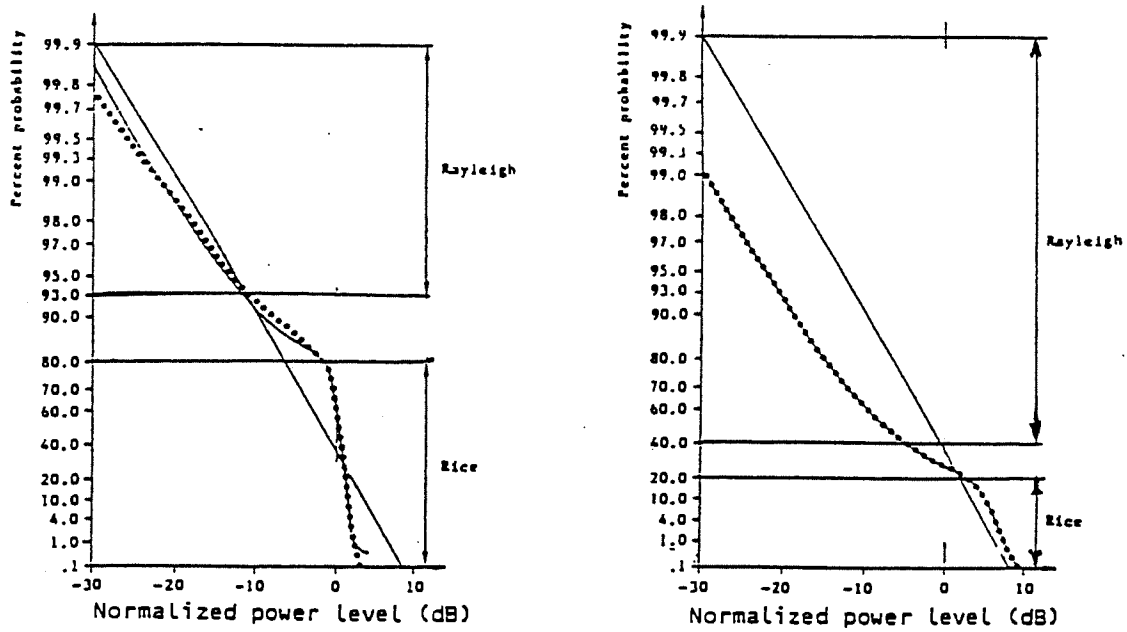

FIGURE 5 - *Complementary cumulative probability distribution function of received power* [Lutz, 1986]

a: Highway, antenna S6
b: City, antenna S6

3. Link margins

For a satellite sound-broadcasting system, the link margins must be carefully specified – they should be neither optimistic nor pessimistic. An optimistic estimate will result in the service quality objective not being met, whereas a pessimistic estimate will needlessly result in the over-design of the satellite. Both of these extremes have substantial cost implications.

Two specific methods for the calculation of the required margins needed to provide a given quality of service are indicated below:

3.1 *Method 1*

Method 1 requires that in a small area the received signal envelope must be above the receiver threshold with probability 0.9:

$$P(r \geq R_0) = 0.9 = \int_{R_0}^{\infty} p(r)\,dr \qquad (9)$$

where

R_0 is the receiver threshold and $p(r)$ is given by equation (4).

It is also required that this condition be met over a larger area with probability 0.9. Invoking the large area probability distribution given in equation (1):

$$P(S_0 \geq \hat{S}_0) = 0.9 = \int_{\hat{S}_0}^{\infty} p(S_0)dS_0 \qquad (10)$$

Where $\hat{S}_0 = \frac{E_0^2}{2} + \sigma_r^2$, which satisfies equation (9).

Equation (9), conditioned by equation (10) can be solved numerically using Marcum's Q fuctions [Brennan and Reed, 1965] or by using the tables supplied by [Nortion et al., 1955]. Bothe methods were used in calculation as a cross check on each other. Equations (9) and (10) were solved to satisfy the given probabilities in terms of $G = \mu + 10 \log (2 \overline{S}_t/R_0^2)$ which is the difference between the large area mean received power and the receiver threshold. Total link margin is given by $L = G - \mu$ (in dB).

Table XXI shows the results of the above calculation for the frequency of 1 GHz and an elevation of 30°.

TABLE XXI

	Urban zone	Rural zone
σ (dB)	3.8	1.2
μ (dB)	-6.4	-1.5
G (dB)	15.4	6.1
L (dB)	21.8	7.6

It should be noted that the values used for σ and μ are average values and are not those applicable to the obstructed visibility case.

The calculated margin of 21.8 dB for the urban area compares with the observed margin of 24.2 dB (translated to 1 GHz) in urban Denver of the United States [Hess, 1980].

It is pointed out that the computed margin depends on the required service quality and coverage. In this example it was assumed that the required service quality was achieved when the signal was above threshold with probability 0.90, and that this condition was to be met with probability 0.90 over the coverage area. Other requirements will lead to different margins.

3.2 *Method 2*

Method 2 requires that the received signal envelope in a given area must be above the receiver threshold (R_0) with probability 0.9. This leads to:

$$P(r \geq R_0) = 0.9 = \int_0^{\infty} \int_{R_0}^{\infty} p(r)p(S_0)dr\, dS_0 \qquad (11)$$

This integral is evaluated numerically using Marcum's Q functions in steps of $G = 10 \log_{10} (2\overline{S}_0/R_0^2)$.

Results are shown in Table XXII, again for the frequency of 1 GHz and elevation angle of 30°.

TABLE XXII

	Urban zone	Rural zone
σ (dB)	3.8	1.2
μ (dB)	-6.4	-1.5
G (dB)	12.0	4.4
L (dB)	18.4	5.9

These calculated values may be compared with measured values. Measurements were made so as to determine the margin as a function of the percentage of locations [Guilbeau, 1979].

4. Frequency selectivity effects

Another important characteristic of UHF radio propagation channel in urban and suburban mobile radio environment is the existence of multiple propagation paths with different and varying time delays. In the case of sound satellite broadcasting, the shortest (direct) path between the satellite and the portable receiver is often blocked by intervening buildings, so that propagation by way of scatter or reflection from buildings around the receiver is significant. Two cases should be considered:

- a stationary receiver; in this case, the radio channel, and thus the propagation statistics of the link, is relatively stable. The multipath propagation characteristics can be described in terms of the multipath spread and correlation bandwidth.

- a moving receiver, the propagation statistics of the radio link is a time-varying function. Different Doppler shifts are associated with scatter paths arriving at the vehicle receiver from different angles. In this context, the key terms are the Doppler spread and correlation time.

The statistical functions which describe the frequency and time selective radio link can be readily obtained by measuring the complex bandpass impulse response of the link. These statistical descriptors and parameter values set bounds on digital communication system performance parameters.

4.1 Delay spread and correlation bandwidth

Consider a statistically stationary channel first. Two spectral components of a modulated signal which are close in frequency will fade in a correlated way, i.e. the two sets of phasors resulting from a given multipath environment will be similar in amplitude and phase. As the frequency separation between the two spectral components increases, the correlation between the two sets of phasors reduces, resulting in amplitude variations (decorrelation) as a function of frequency. This is known as frequency selective fading. The bandwidth at which decorrelation occurs is termed the correlation bandwidth.

The delay power spectrum (also termed as the multipath intensity profile) and spaced-frequency correlation function constitute a Fourier transform pair (Figure 6).

As a result of the Fourier transform, there is a relationship between correlation bandwidth of the statistically stationary channel and of the "delay spread" of the channel:

$$B_c \approx 1/T_o \qquad (12)$$

where B_c is a correlation bandwidth (Hz), and

T_o is a delay spread (s)

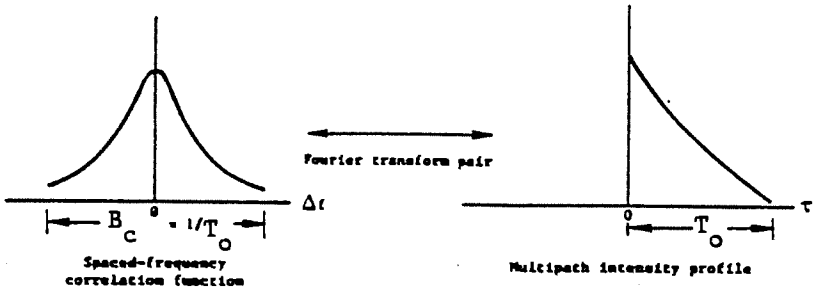

FIGURE 6 - Relationship between T_o and B_c

The delay spread T_o of the channel is a measure of the width of an average power delay profile. Tt is defined as the square root of the second central moment of a profile m [Cox, D.C.,1972].

$$T_o = \left[\frac{\sum_{k=1}^{M} (\tau_k - D)^2 \, P(\tau_k)}{\sum_{k=1}^{M} P(\tau_k)} \right]^{1/2} \qquad (13)$$

where

$k = 1, \ldots, M$ k ranges over the delay axis and M is the index of the last sample along the delay axis

$P(\tau_k)$ an average power delay profile for a set of N consecutive individual profiles

D average excess delay. It is defined as the first moment of the profile with respect to the first arrival delay τ_A:

$$D = \frac{\sum_{k=1}^{M} \tau_k P(\tau_k)}{\sum_{k=1}^{M} P(\tau_k)} - \tau_A \qquad (14)$$

If the correlation bandwidth is small in comparison to the bandwidth of the transmitted signal, the channel is frequency-selective. In this case, the signal is severely distorted by the channel. On the other hand, if the correlation bandwidth is large in comparison to the bandwidth of the transmitted signal, the channel is frequency non-selective.

In order to overcome the selectivity of the channel which may cause intersymbol interference, the delay spread T_o must be much less than the symbol period T_S or, in other words, the delay-spread to symbol-period ratio, i.e. $T_r = T_o/T_S$, should be much less than 1.

The empirical relationship between the correlation bandwidth at 90% correlation and the delay spread (see Figure 7) was obtained from [Cox, Leck, 1975]:

$$B_c\ (90\%) = 90/To,$$

where

B_c (90%) is the correlation bandwidth at 90% correlation between two spectral components (in kHz) and

T_o is the delay spread (in μs).

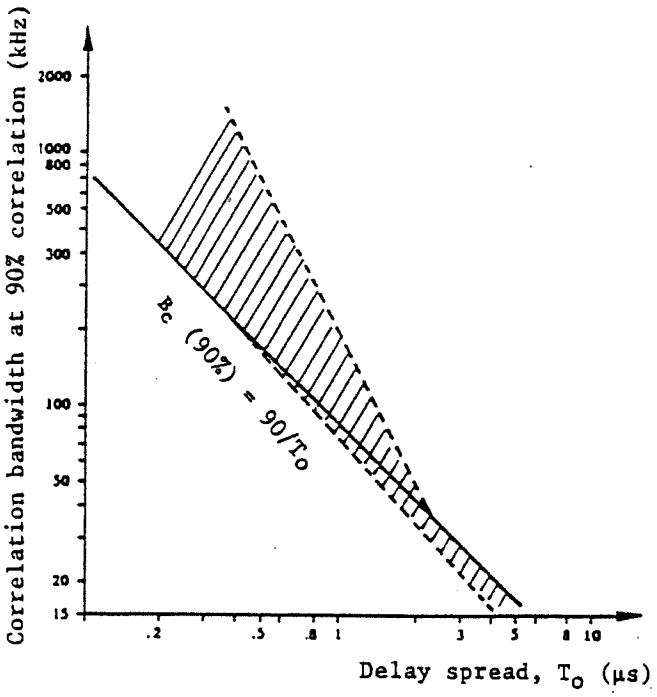

FIGURE 7 - Correlation bandwidth at 90% correlation versus delay spread
[Cox and Leck, 1975]

The corresponding cumulative distribution of delay spreads is shown in Figure 8 below:

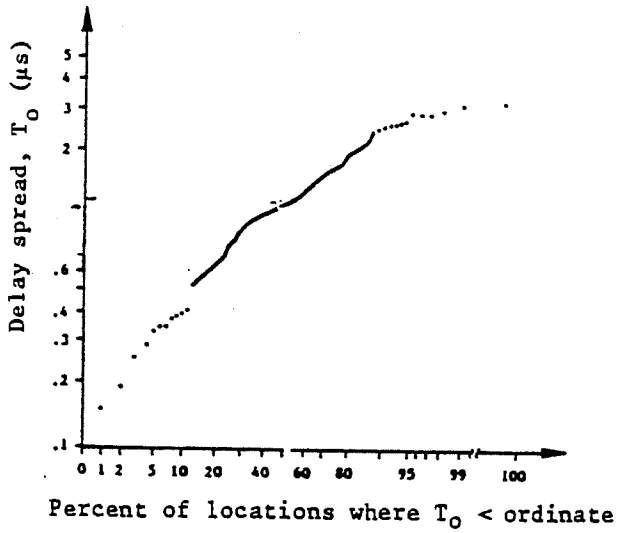

FIGURE 8 - Cumulative distribution of delay spread
[Cox and Leck, 1975]

It can be deduced from the above figure that about 10 percent of small areas have $T_o > 2.5$ μs and about 50% have $T_o > 1.2$ μs.

The corresponding cumulative distribution for B(90%) is depicted on Figure 9 below:

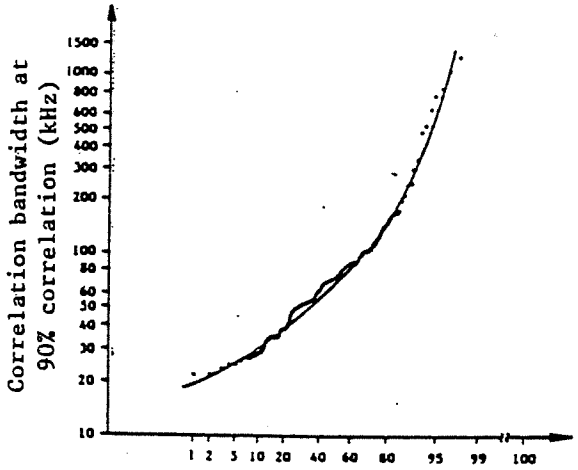

FIGURE 9 - Cumulative distribution of correlation bandwidth at 90% correlation
[Cox and Leck, 1975]

Delay spreads have been measured in residential locations and in a medium sized office building [Devasirvatham, 1986]. The worse case delay spreads of less than 325 ns were obtained when the propagation path followed line-of-sight. When there was no line-of-sight between transmitter and receiver, the delay spread increased up to 422 ns.

Doppler spread and correlation time

In the case of a moving receiver, the time variations of the propagation link result in a Doppler broadening of the received spectrum. If a pure frequency tone is transmitted, a Doppler spread B_d of the channel can be measured.

Analagous to our consideration in the previous section, a measure of the correlation time T_c of the channel could be defined:

$$T_c \approx 1/B_d \qquad (16)$$

where T_c denotes the correlation time (s), and

B_d denotes the Doppler spread (Hz).

A slowly changing channel has a large correlation time and a small Doppler spread. Figure 10 shows that the Doppler power spectrum and the spaced-time correlation function constitute a Fourier transform pair.

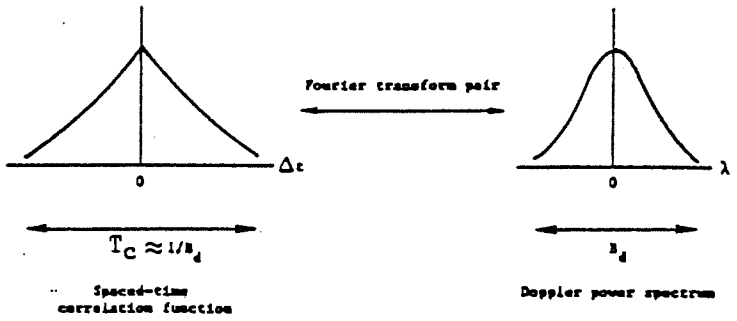

FIGURE 10 - Relationship between B_d and T_c

Fig. 11 shows the averaged signal envelope spectrum obtained during a time period of approximately 1 minute in a suburban area (residential with trees). A distinct frequency cut-off at around 110 Hz is visible in this figure and this value is twice the Doppler frequency f_d given by [Jongejans, 1986]:

$$f_d = v/\lambda = 55 \text{ Hz} \quad \text{for} \quad v = 40 \text{ km/h and}$$
$$f = 1.5 \text{ GHz}$$
$$\varepsilon = 27°$$

This is an indication that in urban environments frequency-spreading of up to twice the Doppler frequency can be expected due to scattering from surrounding obstacles. Thus the Doppler spread B_d equals to 110 Hz.

FIGURE 11 - Spectrum of signal envelope (suburban area); vehicle speed: 40 km/h frequency: 1.5 GHz
[Jongejans, 1986]

REFERENCES

BRENNAN, L. E. and REED, I. S. [April, 1965] A recursive method of computing the Q function. *IEEE Trans. Inform. Theory*, Vol. IT-11, 2, 312-313.

Jongejans, A. et al: PROSAT-phase 1 report, ESA-STR 216, May 1986.

Lutz, E. et al: Land mobile satellite communications - channel model, modulation and error control, Proceedings of ICDSC-7, May 1986, p. 537-543.

Cox, D.C.: Delay Doppler characteristics of multipath propagation at 910 MHz in suburban mobile radio environment. IEEE Transactions on antennas and propagation, vol. AP-20, No. 5, September 1972.

Cox, D.C. and Leck, R.P.: Correlation bandwidth and delay spread multipath propagation statistics for 910 MHz urban mobile radio channels. IEEE Transactions on antennas and propagation, vol. COM-23, No. 11, November 1975.

Devasirvatham, D.M.J.: Time delay spread and signal level measurements of 850 MHz radio waves building environments. IEEE Transactions on antennas and propagation, vol. AP-32, No. 11, November 1986.

Guilbeau, F.: Satellite sound broadcasting on frequencies of about 1 GHz. Simulation of transmission and urban reception. EBU Review - Technical, No. 176, August 1979.

Hess, G.C.: Land-mobile satellite excess path loss measurements. IEEE Transactions on vehicular technology, vol. VT-29, No. 2, May 1980.

NORTON, K. A., VOGLER, L. E., MANSFIELD, W. V. and SHORT, P. J. [October, 1955] The probability distribution of the amplitude of a constant vector plus a Rayleigh-distributed vector. *Proc. IRE*, Vol. 43, 10, 1354-1361.

CCIR Documents

[1978-82]: a. 10-11S/143 (USA); b. 10-11S/176 (ESA); c. 10-11S/177 (ESA); d. 10-11S/10 (EBU); e. 10-11S/29 (USA).
[1986-90]: a. 10-11S/1 (EBU).

ANNEX III

Summary description of advanced digital system I

[CCIR, 1986-90a]

1. Introduction

This annex presents a flexible concept for the implementation of a satellite sound broadcasting system to serve portable and vehicular receivers. The concept is based on the selective use of advanced digital techniques such as convolutional coding, spatial diversity, and Viterbi maximum likelihood decoding. The unique characteristic of this design concept is that varying levels of complexity of the advanced digital technologies are incorporated into different types of receivers only as they may be required by the intended operating environment of the receiver [Miller, 1987]. Thus, to achieve approximately the same overall level of performance, the simplest type of portable receiver operating in high signal-level areas requires only a simple decoder while a vehicular receiver operating in heavily shadowed, rural areas with Rayleigh fading requires quad-spatial diversity, with maximal ratio combining and Viterbi decoding added to provide a very high-quality (Q=4.5), monophonic, sound program channel.

2. Sound coding and modulation

The significant characteristics of the advanced digital satellite sound broadcasting system are given in Table XXII. It is a monophonic or stereophonic sound broadcasting system using adaptive delta modulation with a dynamic range of 85 dB and a sampling rate of 204 ksp/s or 48 ksp/s (kilo samples per second) respectively to provide a measured instantaneous signal-to-noise ratio of at least 58 dB in a 15 kHz baseband bandwidth. Subjectively, at a bit error ratio (BER) of less than 10^{-5} this corresponds to an impairment rating greater than 4.5 (see Report 632-3).

An R=1/2, K=7 convolutional code is used for forward error correction in conjunction with QPSK (4-PSK) and coherent detection with 3 bit quantization at the receiver. Symmetrical phase shift keying is assumed.

TABLE XXIII- Significant characteristics of example advanced digital system I

S/N objective (dB)	58
Baseband bandwidth (kHz)	15
Sound encoding method (ksp/s)	ADM, 204
Forward error correction	Convolutional code, R = 1/2, K = 7
Modulation method	QPSK
RF bandwidth (kHz)	400
Demodulation method	Coherent
Demodulator quantization (bits)	3
Interleaver/de-interleaver	
N	31
M (symbols)	16 384
Decoder	Maximum likelihood, Viterbi decoder with soft decisions
Nominal BER objective	10^{-5}

The combination of QPSK with coherent detection, and the use of interleaved/de-interleaved convolutional forward error correction coding and Viterbi maximum likelihood decoding requires an E_b/N_o of 3.8 dB for an additive white Gaussian noise channel (AWGN) (applicable to portable reception) and an E_b/N_o of 7.4 dB for a memoryless Rayleigh fading channel (applicable to vehicular reception). The use of these techniques provides a coding gain in excess of 37 dB at a BER of 10^{-5} when compared to uncoded transmissions over the Rayleigh fading channel.

The performance given above for forward error correction techniques on the Rayleigh fading channel is based on the assumption that the received symbols undergo independent fading. That is, there is no correlation of the received signal energy from one symbol to the next. One way to ensure that adjacent symbols are uncorrelated is to use an interleaver/de-interleaver pair. This technique is effective for a vehicle velocity greater than a designed minimum value (10 m/s for the example system). Another possible way to mitigate the effects of deep fades on adjacent symbols is to use spatial diversity on the vehicle (two or more antennas) to provide service continuity when the vehicle is stopped [Miller, 1987], see also section 3.

A convolutional interleaver shown in Figure 12 has been chosen for the satellite sound broadcasting application. Synchronization of the de-interleaver is accomplished using a technique proposed by [Viterbi, et al, 1979] and described in [Clark and Cain, 1981]. Referring to Fig.12, a synchronization sequence is added modulo 2 to the coded symbols at the interleaver input and removed modulo 2 by a local estimate of the sequence at the output of the de-interleaver. When the de-interleaver is not synchronized with the interleaver, the synchronization sequence is not removed from the input to the decoder. This results in a BER of 0.5 at the input to the decoder. This condition is easily detected by the decoder and the local estimate of the sync sequence is incremented by one symbol duration. This new estimate is tested and if the BER is significantly less than 0.5, synchronization of the de-interleaver occurs.

The use of the synchronizing sequence has two other advantages:

- it ensures a minimum density of transitions in the transmitted sequence which improves carrier tracking and symbol synchronization at the receiver, and
- it spreads the transmitted power spectral density and will thus facilitate sharing between the broadcasting-satellite service (sound) and terrestrial services.

3. Spatial diversity

Spatial diversity is based on the use of multiple antennas. The antennas must be spaced sufficiently far apart so that the received signals at each antenna fade independently. For a terrestrial mobile system, the required spacing is on the order of one-half wavelength or greater [Lee, 1982]. Comparable spacings are required for space-to-earth paths [Hess, 1980].

The probability of error on a Rayleigh fading, convolutionally coded link that is received with an Mth-order spatial diversity, maximal-ratio combiner receiver and a Viterbi decoder has been evaluated [Miller, 1987]. Table XXIV gives the results of BER calculations for 3rd and 4th order diversity with maximal ratio combining. It is seen that 4th order diversity with a mean bit-energy-to-noise density per branch of about 7.4 dB achieves a BER=10^{-5}.

TABLE XXIV - Probability of error for R=1/2, K=7 convolutional code with Mth spatial diversity and maximal ratio combining
(Eb/No corresponds to the mean bit-energy-to-noise density per antenna)

Eb/No (dB)	Pe (M=3)	(M=4)
2.0	7.821E-03	1.234E-03
3.0	4.295E-03	5.382E-04
4.0	2.318E-03	2.307E-04
5.0	1.232E-03	9.744E-05
6.0	6.478E-04	4.068E-05
7.0	3.373E-04	1.682E-05
8.0	1.743E-04	6.904E-06
9.0	8.948E-05	2.816E-06
10.0	4.572E-05	1.143E-06
11.0	2.327E-05	4.621E-07
12.0	1.181E-05	1.863E-07
13.0	5.976E-06	7.488E-08
14.0	3.018E-06	3.004E-08
15.0	1.522E-06	1.203E-08
16.0	7.667E-07	4.814E-09
17.0	3.857E-07	1.924E-09
18.0	1.939E-07	7.684E-10
19.0	9.744E-08	3.067E-10
20.0	4.893E-08	1.223E-10

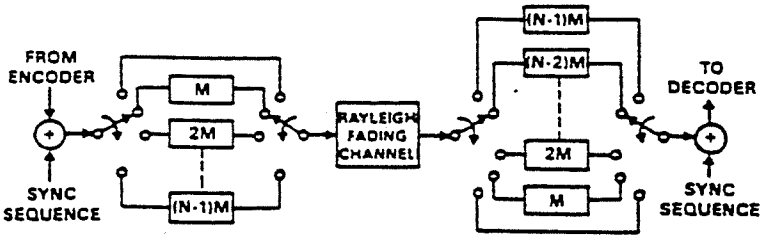

FIGURE 12 - Shift register implementation of the convolutional interleaver/de-interleaver

REFERENCES

Miller, J.E. [June 1987] Technical Possibilities of DBS Radio At or Near 1 GHz, 15th International Television Symposium and Technical Exhibition, Montreux, Switzerland, pp 387-405

VITERBI, A.J., ODENWALDER, J.P., BAR-DAVID, I., and KUMM, K.M., [January, 1979] RFI/Coding analysis for tracking and data relay satellite system (TDRSS), Phase II Final Report. Linkabit Corp.

CLARK, G.C. Jnr., and CAIN, J.B., [1981] Error-correction coding for digital communications, 345-352. Plenum Press, New York and London.

LEE, W.C.Y. [1982] Mobile Communications Engineering, McGraw-Hill Book Co. New York, London, etc.

HESS, G.C., [May 1980] Land-Mobile Satellite Excess Path Loss Measurements, IEEE Transactions Vehicular Technology, Vol. VT-29, No. 2, pp 290-297

CCIR Documents

[1986-90]: a. 10-11S/52 (United States of America).

ANNEX IV

SUMMARY DESCRIPTION OF ADVANCED DIGITAL SYSTEM II

[CCIR, 1986-90a, b, c]

1. Introduction

The purpose of this annex is to describe a new sound radio broadcasting system specifically adapted to channels impaired by multipath distortion. The general philosophy consists in breaking down the information to be transmitted into a large number of low bit rate elementary sub-channels, which turns a highly selective wideband channel into a large number of unselective FDM narrow-band channels. This solves the intersymbol problem by increasing the symbol time in the ratio of the number of sub-channels.

Combined with this FDM narrow-band transmission technique, the use of a convolutional coding system suited to the fading character of the channel substantially enhances the performance obtained. In a Rayleigh selective channel the performance in terms of E_b/N_o for a given bit error ratio approaches that for a Gaussian channel to within about 2 dB using the same channel coding scheme.

2. Signal description

The transmitted signal is a Coded Orthogonal Frequency Division Multiplex (COFDM) using equally spaced and mutually overlapped carriers. [Pommier and Wu, 1986; Alard and Lassalle, 1987.] With this arrangement each carrier is an element of a Discrete Fourier Transform of the overall transmitted signal (Figure 13). The receiver as well as the transmitter structure is then based on the use of a Fast Fourier Transform (FFT) algorithm. The multiplexing of the sound channels should be chosen to permit reduced receiver complexity when each given service occupies only a part of the total capacity. Indeed, as the receiver has then to deal only with a part of the transmitted data multiplex, the basic idea is to arrange the coding and modulation such that one given part of the data multiplex can be processed separately from the others. This can be done by either a frequency or a time division multiplex. When the frequency division multiplex is used, programme selection and demodulation can then be effected by decimation of the FFT algorithm so as to restore the wanted programme. In both cases, receiver tuning and demodulation are therefore entirely digital.

3. Use of a guard interval

With the COFDM technique the selectivity effect of the channel is largely reduced in proportion to the number of carriers. An additional provision against intersymbol interference is taken by transmitting symbols of a period greater than the nominal value. This additional guard interval absorbs all the intersymbol interference generated by any delay spread ranging from 0 to the guard interval duration.

4. Channel coding

A convolutional code processed with soft decision is used in conjunction with a two dimensional interleaving:

- time interleaving, which is useful with mobile reception;
- frequency interleaving, which is essential for this system in urban environments, for fixed reception and stationary vehicles.

Figure 14 shows the error rate as a function of the mean E_b/N_o ratio in a frequency selective channel of which the correlation bandwidth (see also Annex II) is small in comparison to the bandwidth of the transmitted signal and where the COFDM technique is used. Curves show the performance with convolutional coding ($R = 1/2$, $k = 7$, $D_{free} = 10$) for 2PSK and 4PSK with differential and coherent demodulation compared to that of the uncoded system. The COFDM modulation technique using convolutional codes effectively solves the frequency selective fading problem.

5. Source coding

Digital sound broadcasting requires significant bit-rate reduction of audio signals while preserving excellent quality of the sound. Recent progress in source coding techniques has made available coding and decoding procedures that allow bit-rate reductions from 16 bit/sample as currently used in digital audio equipment to about 2 bit/sample; using a sampling frequency of 48 kHz, the total bit rate of a monophonic signal is around 100 kbit/s.

In order to match the quantizing noise to the human ear characteristics, two different source coding techniques are under investigation. They both use spectrum analysis techniques and frequency-dependent bit-allocation. The goal of these advanced coding schemes is to give compact disc quality and the preliminary results have shown that this goal is likely to be achieved.

5.1 Transform coding

This coding method involves the conversion of a block of consecutive samples into the frequency domain <Krahé, 1986, Brandeburg, 1988, Johnston, 1988> (e.g. Fourier transform or cosine transform). This strategy enables a reduction in the redundancy of the audio signal and also a matching of the quantization to the thresholds of perception of quantizing errors. Only those values of amplitude and phase that are relevant with respect to the masking effects of the human ear are quantized.

5.2 Sub-band coding

This coding method divides the broadband signal into a number of sub-band signals with a suitable filter bank and into digital frames of about 4 to 10 ms long <Theile et al., Dehery, Vörös, 1988)>. In each frame, the maximum level attained by each sub-band signal (i.e. the scale-factor) is quantized and transmitted. Each sub-band is quantized with the bit-allocation based on the masking thresholds. This method avoids problems with time domain windowing and whatever the dynamic range of the input signal, it optimizes the distribution of the quantizing noise across the spectrum with regard to the perceptibility. Sub-band coding is characterized by an inherent low sensitivity to transmission errors because the spectrum of the noise energy is confined to a single sub-band and is limited by the scale-factor if this one is satisfactorily protected.

In the sub-band coding, the basis for dynamic bit-allocation to the sub-bands is an exact calculation of the instantaneous masking threshold in the coder. The bit-allocation control data are transmitted together with the scale-factors as side-information. Thus the complexity of the decoder is reduced to inverse filtering operation. This technique gives a constant bit rate by providing optionally a dynamically varying bit-rate margin, which can be used, for instance, to transmit arbitrary data.

6. System considerations

The very first realization has been developed in France to validate the system principles. It offers a capacity of 16 stereophonic sound programmes, each with an individual capacity of 336 kbit/s, in an overall bandwidth of 7 MHz.

Nevertheless, the results already achieved in audio data bit-rate reduction and the assurance, based on the knowledge of the channel behaviour, that a 4 MHz band is sufficient to provide an excellent quality, led to two sets of representative system parameters for the link budget:

- system A, which transmits 16 stereophonic programmes each with an individual source bit rate of 168 kbit/s, in a 4 MHz band;
- system B, which transmits 12 stereophonic programmes each with an individual source bit rate of 224 kbit/s, in a 4 MHz band.

The existing realization described below has a capacity of 33 channels (C0 to C32). The channel C0 can be used for data broadcasting. Channels C1 to C32 are nominally allocated to sound broadcasting. Each one can transmit a high-quality monophonic sound compressed at 168 kbit/s, a rate that includes program-related data. The general architecture of the system is shown in Figure 15.

6.1 COFDM/4PSK modulation system

The basic parameters for the first version of the COFDM system are as follows:

Symbol duration	$T_s = 80\ \mu s$
Useful period	$t_s = 64\ \mu s$
Guard interval	$\Delta = 16\ \mu s$

The 16 μs duration of the guard interval absorbs multiple paths in almost all practical situations. Loss due to the guard interval amounts to approximately 1 dB. In addition, symbol T_s is of sufficiently short duration to ensure temporal coherence in the received signal, even at mobile receiver speeds of approximately 200 km/h and an operating frequency of 2 GHz. This condition is vital if the demodulator is to function correctly, whether it is of the differential or, a fortiori, of the coherent type.

The multiplex consists of 448 carriers spaced by $1/t_s$, i.e. 15625 Hz. The resulting bandwidth is approximately 7 MHz. Each of the carriers is modulated in 4-PSK with differential coding. This allows for simplified receivers based on differential demodulation.

6.2 Frame organization

Time Division Multiplex is based on a frame of 300 symbols, or time slots, i.e. 24 ms, as shown in Figure 16. The first slot in the frame is always set to zero and is used for receiver synchronization. The second slot is a frequency sweep used as a phase reference for differential demodulation. The third slot transmit static data. The remaining 297 slots are divided out between the 33 channels, each channel having nine consecutive slots.

6.3 Channel coding system

The channel coding retained is of the convolutional type. For each channel, a block is formed corresponding to the data transmitted in one frame, i.e. 24 x 168 = 4032 bits. The convolutional code has a rate 1/2 and a constraint length k = 7, forming an 8064 bits block at the output. The data from the convolutional coder are then interleaved in time over 16 frames, i.e. 384 ms. Frequency interleaving spreads the data over the 448 carriers of the multiplex.

6.4 Diversity techniques

The diversity techniques play a vital rôle in the system. The convolutional code cannot function correctly in a Rayleigh channel unless independent Rayleigh laws have been allocated to the successive samples presented to the Viterbi decoder. As shown in Section 6.3, the temporal interleaving extends over 384 ms, which, in the case of frequencies of the order of 500 MHz to 2 GHz, provides the necessary independence even when the vehicule is travelling at very low speeds. When the vehicle stops, then the frequency diversity alone ensures that the system functions correctly. From this point of view, the existence of multipath propagation is a form of diversity and should be seen as an advantage for this system.

6.5 Source coding system

The prototype implementation of an advanced source coding system called MASCAM (Masking Adapted Sub-band Coding And Multiplexing) was developed in Germany (Federal Republic of). It used a sampling frequency of 32 kHz and a static bit-allocation. Further work has been carried out in European research centres [Theile et al., Dehery, 1988] in order to optimize a 48 kHz sub-band coding scheme with a view to establish the best trade-off as regards subjective quality, bit-rate, delay, bit-error ruggedness, decoder complexity and post-processing capability. The studies have been oriented in two directions:

- redesigning the characteristics of the sub-band analysis and synthesis filter bank in order to improve the corresponding spectral analysis and quantizing noise confinement property and in addition try to reduce the overall coding-decoding delay;

- applying a dynamic bit-allocation, based upon an exact calculation of the masking threshold. The resulting bit-rate for transmitting an audio signal providing a subjective quality of 16 bit linear could in such a case be reduced to less than 100 kbit/s per monophonic channel.

The block diagram of the new coder using a sub-band coding scheme is shown in Figure 17. Further information on advanced source coding schemes is given in Report [Study Group 10].

7. Receiver design

The general architecture of the receiver is shown in Figure 18.

7.1 RF, IF and baseband

The receiver input stages are totally conventional in the RF stages. In IF, channel filtering is performed by a SAW filter with a bandwidth of 7.5 MHz. The IF signal is then demodulated and the signals I and Q are converted into digital form. Note that the local oscillator corresponds to the center of the channel. In order to avoid any mixer isolation problems, the carrier corresponding to this frequency is not emitted.

7.2 Demodulation of the COFDM multiplex

The incoming signal is demodulated by a processor which performs a 512 complex point FFT in about 1 ms. This allows for the processing of two elementary channels in a real time, i.e. one stereophonic sound. The 448 useful carriers are then demodulated differentially using complex multiplication.

7.3 Viterbi decoding

The Viterbi decoding function is performed by a custom designed integrated circuit which provides for a large range of codes among which is the $R = 1/2$, $k = 7$, $D_{free} = 10$ code, and can process a maximum useful rate of the order of 500 kbit/s.

7.4 Synchronization

Synchronization is performed digitally by measuring the energy received and detecting slot 0. This first estimate provides a mean of prepositioning the FFT window. This positioning is then refined by a channel impulse response estimation.

7.5 Sound decoder

The sub-band decoder (Figure 19) is characterized by inverse transcoding and by inverse filtering of the sub-band samples. For inverse transcoding the allocation control and the scale factors are used.

The computation power required by the decoder is significantly less compared to the coding process and is mainly determined by inverse filtering, characterized by simple structures which can be easily implemented in a special VLSI.

8. Experimental results

The remarkable performance of the system has been particularly confirmed by the first demonstration of COFDM/MASCAM, which was organized under EBU's auspices during the WARC ORB-88 in Geneva [Ch. Dosch et al., 1988].

The COFDM/MASCAM signal transmitted at 834 MHz from the top of the Mont Salève was received in a demonstration car travelling in the streets of Geneva. The quality of the transmission monitored both on loudspeakers and headphones was excellent, even when the car was shadowed by the buildings and in strong multipath conditions.

The modulation and source coding parameters of the experimental system are given in Tables XXV and XXVI, respectively.

The subjective quality of the sound received in the car was evaluated after the demonstrations on the basis of the replies to the questionnaires given to the delegates.* 70% of all participants could not detect any interruptions at all during the 20 minute ride. Only 30% of the participants noticed one to four disturbances, such as clicks, short beeps or brief mutings. All participants judged the sound quality as more then adequate. 80% of the participants evaluated the overall performance as "excellent" (i.e. grade 5), and no passenger assessed it worse than "good" (i.e. grade 4).

TABLE XXV

System parameters of the first implemented version of COFDM

Total number of carriers processed by FTT		512
Total number of useful transmitted carriers		448
Spacing between two successive carriers		15625 Hz
Useful symbol period		64 μs
Total bandwidth		7 MHz
Modulation		4 PSK
Interleaving:	- time domain	(not implemented in Geneva demonstrations)
	- frequency domain	7 MHz
Demodulation		differential
Channel coding		convolutional code
	- rate	1/2
	- constraint length	7
	- free distance	10
Channel decoding		maximum likelihood Viterbi decoder
Total useful bit-rate		5.5 Mbit/s
Number of stereophonic sound programmes		16

* More than 200 delegates attending WARC ORB-88, from 40 countries, participated in a test drive in the car.

TABLE XXVI

System parameters of the first implemented version of MASCAM

Bit-rate per mono channel	- Total bit-stream	168 kbit/s
	- Samples	112 kbit/s
	- Scale-factors	24 kbit/s
	- Error protection	32 kbit/s
Number of sub-bands		24
Width of sub-bands		500 Hz (up to 8 kHz) 1 kHz (above 8 kHz)
Sampling rate		32 kHz
Block length		8 ms (below 8 kHz) 4 ms (above 8 kHz)
Code-words per block		8 samples
Length of samples		1.56 to 12 bit/sample depending on the sub-band location
Scale-factor length		6 bits
Error protection	- Block code	Golay (24,12) covering scale-factors of all sub-bands - 2 MSB of sub-bands Nos. 1 and 2 - 1 MSB of sub-bands Nos. 3, 4 and 5

9. References

CCIR Documents

[1986-1990]: a. 10-11S/9 (France);
b. 10-11S/2 (EBU);
c. 10-11S/122 (EBU)

Pommier, D., Wu, Y. <June 1986>: Interleaving or spectrum-spreading in digital radio intended for vehicules. Reprinted from the EBU Review-Technical No. 217

Alard, M., Lassalle, R. <August 1987>: Principles of modulation and channel coding for digital broadcasting for mobiles receivers. Reprinted from EBU Review- Technical No. 224

Theile, G., Stoll, G., Link, M. <August 1988>: Low bit-rate coding of high-quality audio signals. An introduction to the MASCAM system. EBU Review-Technical No. 230, pp. 158-181

Dehery, Y.F. <August 1988>: Real-time software processing approach for digital sound broadcasting. In: Advanced digital techniques for UHF satellite sound broadcasting. EBU publication, pp. 95-99

Vörös, P. <April 1988>: High quality sound coding within 2.64 kbit/s using instantaneous dynamic bit-allocation. Proc. ICASSP, New York, pp. 2536-2539

Krahé, D. <1986>: Ein Verfahren zur Datenreduktion bei digitalen audio-signalen unter ausnutzung psychoakustischer phänomene. Rundfunktechnik Mitteilungen 30, pp. 117-123

Brandenburg, K. <1988>: High quality sound coding at 2.5 bit/sample. 84th AES Convention, Preprint No. 2582

Johnston, J. <February 1988>: Transform coding of audio signals using perceptual noise criteria. IEEE Journal on selected areas in communication, Vol. 6, No. 2, pp. 314-323

Dosch, Ch., Ratliff, P.A., Pommier, D. <December 1988>: First public demonstrations of COFDM/MASCAM. A milestone for the future of radio-broadcasting. EBU Review-Technical, No. 232, pp. 275-283

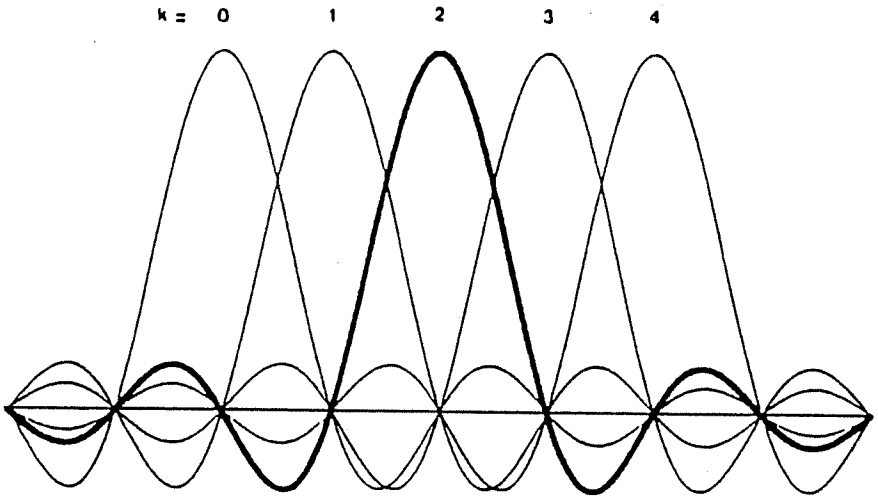

FIGURE 13

Spectrum of the COFDM elementary carriers

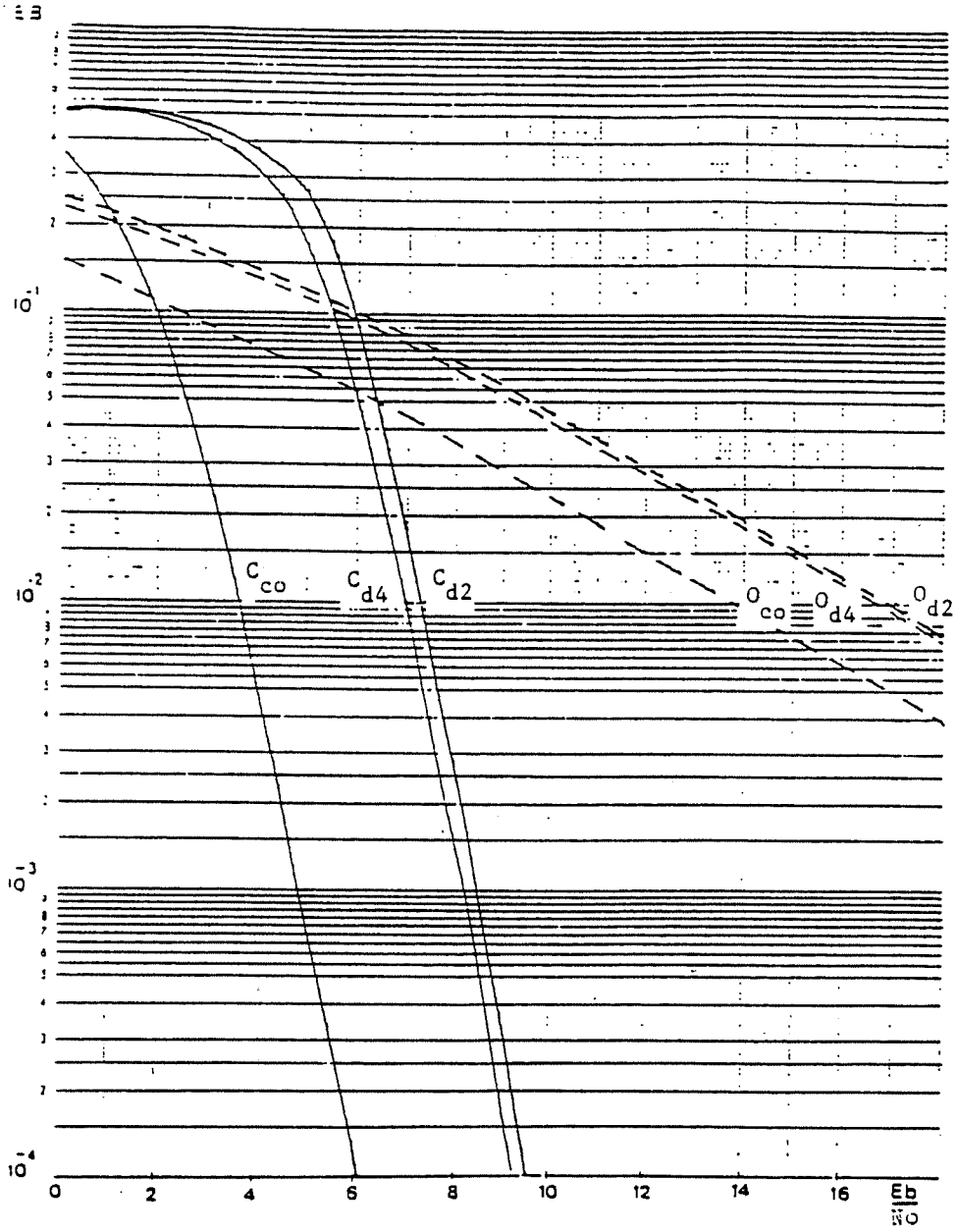

C convolutional code

O no coding

co coherent demodulation

d2 differential demodulation (2PSK)

d4 differential demodulation (4PSK)

FIGURE 14

Comparison of binary error rate performance of convolutional code with COFDM in a Rayleigh channel using coherent and differential demodulation (2PSK, 4PSK)

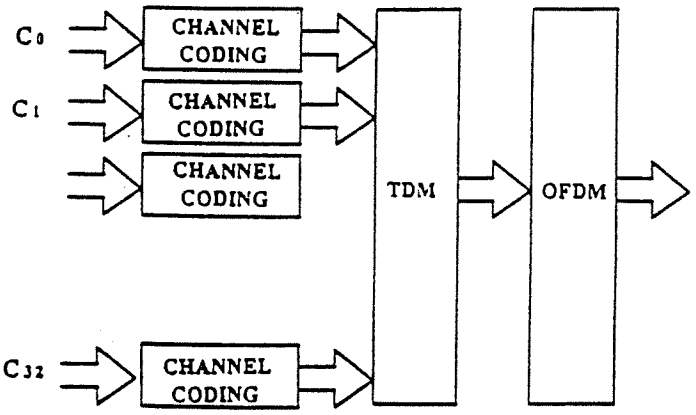

FIGURE 15

Schematic diagram of coding system

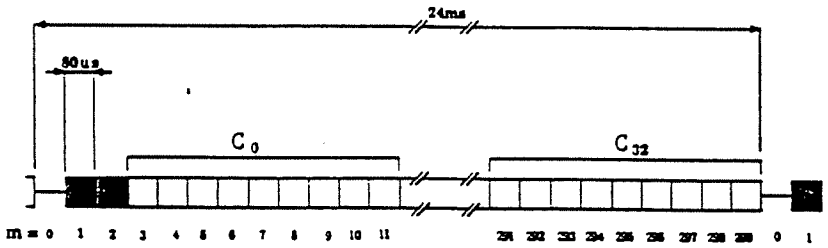

FIGURE 16

Frame structure

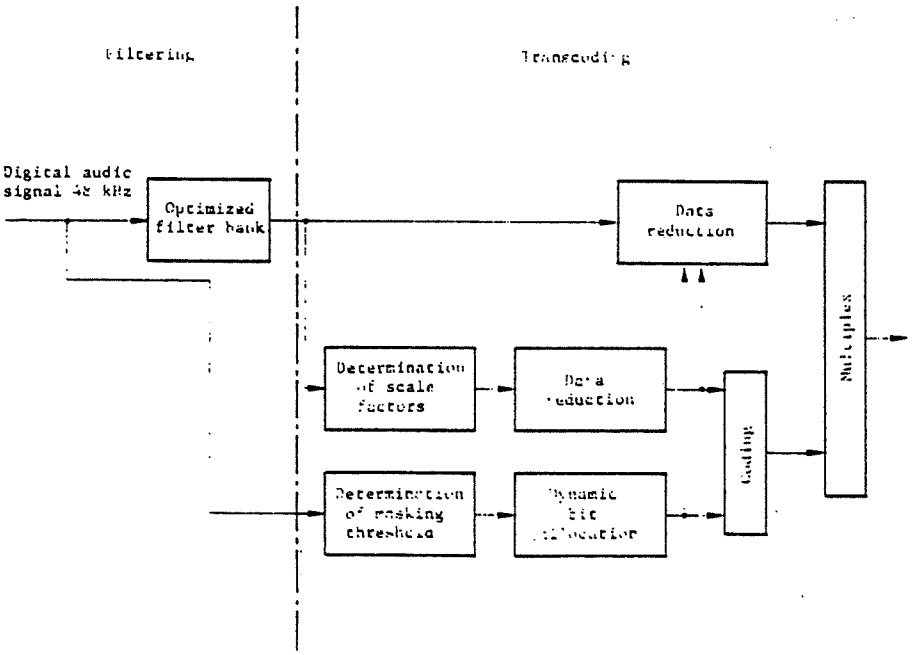

FIGURE 17

Block diagram of an optimized sub-band coder

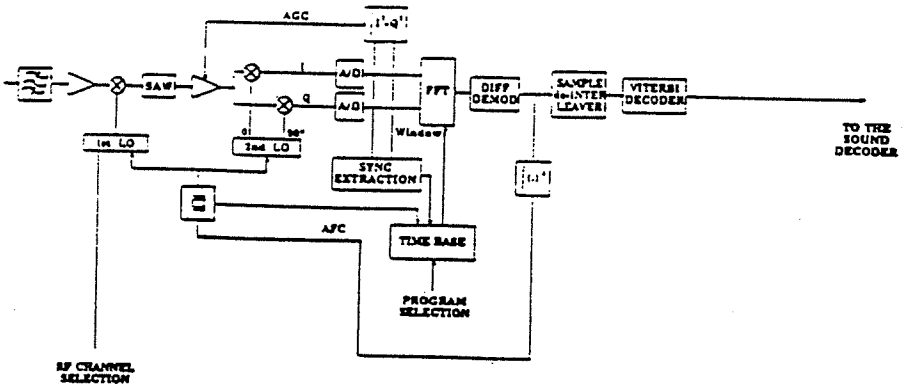

FIGURE 18

Block diagram of the receiver

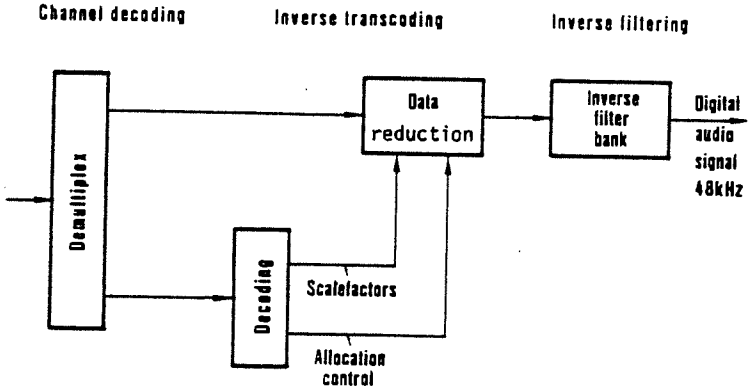

FIGURE 19

Block diagram of the sub-band decoder